# Analysis of various spectral indices and their weighted fusion techniques for the accurate extraction of forest burn scar in tropical deciduous forest

**Amrita Singh, A. O. Varghese, Jugal Kishore Mani, Ashish Kumar Sharma and G. Sreenivasan**

Regional Remote Sensing Centre-Central, NRSC, ISRO, Amravati Road, Nagpur, Maharashtra-440033, India

Corresponding author: Amrita Singh, email-amrita.singh1410@gmail.com

**Abstract**

The recurrent occurrence of fire is one of the most complex problems facing in deciduous forests in tropical regions, adversely impacting the ecology, atmospheric systems, as well as on living environment. Detecting and assessing the exact spatial extent and distribution of burn scar can support forestry services in pre & post fire management. Exact mapping of forest fire scar can also lead to assessing forest fire frequency, severity, risk zones and identification of suitable area for watchtowers and fire and grazing closure areas. In the present study, tropical deciduous forests of Vidarbha region of Maharashtra, India is taken as study area. Burn scar detection and discrimination capabilities of seven widely used Spectral Indices (SI) such as Burn Area Index (BAI), Burned Area Index Modified-lSWIR (BAIML), Burned Area Index Modified-sSWIR (BAIMS), Normalized Burn Ratio (NBR), Normalized Difference Vegetation Index(NDVI), Normalized Difference Moisture Index(NDMI), Modified Soil-Adjusted Vegetation Index (MSAVI) and their weighted fusion were examined in multi-temporal domain. This study created difference images during fire season using individual SI, change vector analysis (CVA) and weighted fusion normalized difference image technique. Comparative analysis was performed between these approaches towards their capability for burn scar discrimination with M statistics, burn & unburn class distribution and descriptive evaluation of confusion matrix. The study demonstrated that Weighted Fusion of BAI, MSAVI and BAIMS is more accurately discriminating burn scar and offers a very low rate of omission (9.27%) and commission (4.12%) errors with good overall accuracy (86.61%) amongst other examined individual SIs and their ensembled images.



**Key words:** Forest fire, burn scar extraction, spectral indices, weighted fusion, change vector analysis

## 1 Introduction

Forest fire in India is largely of anthropogenic origin rather than natural. Forest fire, or we should categorize it as uncontrolled wildfire, caused extensive quantitative and qualitative damage to forest ecosystem and seriously threatened its flora and fauna[1,2]. Burn scar can be defined as areas damaged by uncontrolled burning (such as forest fire, grass fire etc.) and controlled burning and have not yet recovered[3]. Usually, the controlled fire is ignited by the forest-dependent communities for various purposes ranging from clearing community forests for shifting cultivation to clearing the forest floor to encourage grass growth and the collection of non-wood forest produce. On the other hand, uncontrolled and unmanaged fires cause remarkable negative impact on biodiversity, structure and composition of the forest[4]. Forests of our country are prone to fires and getting impacted with varying intensity and extent. Based on the forest inventory records, 54.40% of forests in India are exposed to occasional fires, 7.49% to moderately frequent fires and 2.40% to high incidence levels, while 35.71% of India's forests have not yet been exposed to fires of any real significance[5]. Every year 2-5% of forests are affected by fires that damage their precious ecological resources. Due to the severe forest fires, forest ecosystem can get affected by irreparable damages. Escalated anthropogenic activities due to population increase and climate changes are the leading cause of the increased frequency as well as intensity of forest fires[6,7]. Considering these, India has to put more focus on strengthening its efforts for efficiently managing the forest fires to achieve its goals set for green India[8]. A large variation exists between exact area burnt and area reported by ocular method by the forest staff. Most of times the area reported are less than reality or sometimes highly exaggerated as the estimation technique is ocular without surveying in detail. An average of 17% error is present between the ground and reported areas[9]. In general, burn area has the properties of large size and spatial variability. The advantage of wide viewing angles, multi-spectral imaging and multi-temporal revisit capabilities of satellite remote sensing technique qualify it as a primary tool for burn scar

extraction. Using geospatial technology in forest fire management will minimize work, cost and higher accuracy[10]. However, most of the forest fire information available online in the Indian region are point location information on active fire and fire susceptibility[11,12]. Also, the information on forest burnt area and fire frequency using satellite remote sensing data is not available[5]. Currently, most of the techniques developed internationally to derive burn scar information from satellite remote sensing data have been commonly applied to specific fire events. Also, the major estimation is based on coarse resolution sensors and is likely to be a conservative estimate of total burned area (BA). Some of the studies which were undertaken for forest burn scar assessment using spectral indices are based on NBR[13, 14], NDVI[15], NBR & NDVI with machine learning (ML) technique[16,17,18] and NDVI, NBR & RBR[19]. Many studies used ML techniques with various spectral indices[20,21] and object-oriented methods[22]. The capability of the individual spectral index and the combination of these spectral indices in forest fire scar delineation is not attempted. By taking the advantage of SI or their combinations, whoever is demonstrating the best delineation of burn scar, proper samples for ML can be created which is vital to get an accurate output from any ML techniques. This study with a medium-resolution sensors may increase the knowledge about the discrimination capabilities of different SI indices in the estimation of burn scars in tropical deciduous forests. Here, Landsat-7 and Landsat-8 satellite images have been used for burn scar extraction. Comparative analysis has been performed between difference images generated using individual spectral indices and ensemble spectral indices to come up with the best suited method for exact discrimination of burn scar. The result of exact spatial extent and distribution of burn scar can support forestry services to reduce forest fire occurrences, which entails pre-fire and post-fire management. As per the National Working Plan code-2014 (for sustainable management of forest and biodiversity in India) year wise spatial extent of fire and frequency assessment using satellite imageries has become mandatory for working

plan preparation. The outcome of this study can support in identifying the fire closure and regeneration areas and can also be used in designing fire lines in working plan preparation.

## 2 Materials and Methods

### *2.1 Study area*

Vidarbha region of Central India is taken as study area for burn scar analysis (Figure 1). The climate of this region can be classified as semi-arid and is richly endowed with natural resources of varied types. The region consists of eleven districts viz., Buldana, Akola, Washim, Amravati, Yavatmal, Wardha, Nagpur, Bhandara, Gondia, Chandrapur and Gadchiroli. It is situated in between 17°57'-21°46' N latitude and 75°57'-80°59′ E longitude and covers an area of 98 lakh ha, which is 32% of total area of Maharashtra. The mean annual rainfall ranges from 700 mm in the west to 1700 mm in the east. This region mostly receives adequate rainfall in aggregate during monsoon period but suffers from vagaries of distribution and, consequently, scarcity and semi-scarcity conditions. Vidarbha region has been divided into three agro-climatic zones based on rainfall, soil types and vegetation viz., western Vidarbha Zone (Rainfall: 700 to 950 mm), Central Vidarbha Zone (Rainfall: 950 to 1250 mm) and Eastern Vidarbha Zone (Rainfall: <1250 mm). Vidarbha region forests are mostly tropical deciduous forest consists of *Tectona grandis*, *Artemisia pallens*, *Dalbergia sissoo*, *Diospyros melanoxylon*, *Butea monosperma*, *Aegle marmelos*, *Senegalia catechu*, *Hardwickia binata* etc. Some pockets of hilly regions have tropical thorn forests consists of *Acacia*, *Senegalia catechu*, *Acacia leucophloea* trees.

**Figure 1**



### *2.2 Data used*

Vidarbha region is located in Central India. The forests of the study area are primarily dry deciduous forest, frequently affected by forest fires. Annually, wildfire crop up from February to June

in summer months, but in some scenario, November to January is also considered fire season[9]. In the present study, December to May have been considered as fire season, and for these six months, possibly for the last week of the month, temporal Landsat-8 and Landsat-7 satellite data have been downloaded from Dec. 2017 to May 2018 from USGS website (https://earthexplorer.usgs.gov/) to maintain minimum 20 to 30 days gap between consecutive months' images. During the fire season, ten scenes per month of Landsat ETM+/OLI satellite data were required to cover complete study area with minimal cloud coverage. During scene selection, priority was given to Landsat-8 as landsat-7 data needs scan line removal before further processing. While selecting scenes, proper care has been given to consider the proper similarity with respect to sun elevation and sun azimuth. Nearly 258 polygon data with varying degree of fire scar were collected from the field for ground truth information. Out of 258 polygons, 112 were burnt patches of different sizes and 146 were unburnt patches of various aspects. The collected ground truth data were used as inputs for threshold calculation, separability analysis and classification validation.

### *2.3 Methodology*

The overall methodology is represented in the following flow diagram (Figure 2).

**Figure 2**

#### *2.3.1 Data pre-processing*

In order to extract burn area more conveniently and accurately, the prerequisite is that the data should be cloud free as much as possible because cloud shadow, being the low-reflectance target, is one of the potential confusion sources with burned areas. For remaining cloud patches, masking the cloud and its shadow was performed using cloud masking plug-in in QGIS. All Landsat-7 scenes have scan line error, which is no data and was fixed using QGIS software. Normalisation of multispectral data was performed through top-of-atmosphere correction, which gives the surface

reflectance value of each pixel after removing atmospheric effect caused by different gases, aerosol, etc. To cover the full extent of the study area, in each month of fire season, band wise, ten scenes were mosaicked. Further, a forest mask was generated with each band scenes to exclude all non-forest areas, which can produce potential confusion with burned areas[8,23].

### *2.3.2 Description of spectral indices (SI)*

The present study selected seven different spectral indices among the wide range of existing spectral indices commonly used worldwide for burn scar identification and extraction, as listed below (Table 1):

**Table 1**

### *2.3.3 Approach*

As fire destroys the vegetation cover of forest and its moisture conditions, the spectral indices (SIs) sensitive to these will get changed its reflectance after the fire[31]. This essential phenomenon of SIs has been utilised in this study. At first, month wise (during fire season), seven spectral indices are generated, and the outcomes are visually compared with satellite image and ground truth/fire hotspot locations. The results found individual indices unsuitable for burn scar extraction as these results carry many spectral mixing (hilly shadows, water logged or wetland condition etc.) having very similar reflectance properties as burn scar. Hence, the difference image technique has been adopted. For comparing the bi-temporal images taken over the same geographical area at different dates, difference image is the first step carried out for the comparison between pre-fire and post-fire images. This practice enhances the recognition characteristics of any feature of interest, which in this case is burn scar[32]. Also, it reduces the effect of some unwanted spectral confusion, like a hilly shadow. As, the proposed method is trying to remove dependency on specific fire events and not leave any burn scar unattempted. So each month, possibly for the last week, one Landsat dataset has been

downloaded, and consecutive months' images with a gap of 20 to 30 days are considered pre- and post-fire images for difference image generation. For January, the December image is taken as a pre-fire image; for February, the January image is taken as a pre-fire image, and so on. As, burnt pixels present in the indices NDVI, NDMI, NBR, and MSAVI have lower (darker) reflectance values, unlike indices like BAIMS, BAIML, and BAI, which demonstrate higher (brighter) reflectance values. All indices burned pixels representations are brought to same at lower (darker) reflectance value by (inverting the difference image values of BAIMS, BAIML, and BAI) calculating difference image as post fire – pre fire for NDVI, NDMI, NBR and MSAVI and prefire – postfire for BAIMS, BAIML and BAI.

The present study generated the final difference image via combining weighted features of difference images of individual spectral indices and change vector analysis (CVA) image. SI difference images and CVA images were created by considering each consecutive month's scenes as pre- and post-fire images to capture the change occurred month wise. The CVA principle defines the difference of single feature across various bands between two dates, which exhibits the change of pixels in individual band. CVA image can be calculated as (Equation 1)[1].

$$\mathbf{CVA} = \sum_{k=1}^{n} \left[ \boldsymbol{BV}_{ijkdate2} - \boldsymbol{BV}_{ijkdate1} \right]^2 \qquad (1)$$

Where, CVA describes spectral difference of two remote sensing images captures at different dates by applying CVA algorithm. BVijkdate1 and BVijkdate2 are the kth band value of pixel located at (i, j) corresponding to pre-fire and post-fire images respectively. k= 1,2, 3….n, and n is the number of remote sensing image bands.

Then, ensembling different set of these SI difference images and/or CVA month wise weighted fused normalized difference images were obtained (Equation 2). Standard deviation of CVA and each selected SI difference images for the respective ensembling was taken as weight value[3].

$$\mathbf{DI} = \frac{D_{SI1}}{\sigma_{SI1}} + \frac{D_{SI2}}{\sigma_{SI2}} + \cdots + \frac{D_{SIn}}{\sigma_{SIn}} + \frac{CVA}{\sigma_{CVA}} \quad (2)$$

Where, DI is the weighted fusion difference Image, DSI is the difference image calculated by selected SI feature, CVA is the difference image acquired according to CVA algorithm, coefficient σSI and σCVA is the standard deviation of the selected difference images and n varies from 2 to selected number for ensemble.

After difference image calculation, month wise burn scar extraction using optimal thresholding was performed on the difference images obtained from individual spectral indices, CVA and features weighted fusion technique. Threshold for individual difference images were computed based on ground truth samples. After applying threshold, image smoothing is performed to remove unwanted isolated pixels, for this, at first, individual unique zones was created for each cell. Then, a defined filter is applied to omit the regions from the image that are less than a certain number of pixels.

***2.3.4 Best method identification for burn scar delineation***

To access the best suited method for exact detection and delineation of burn scar, a comparative analysis of these SI difference/weighted fusion difference images were performed to estimate their effectiveness towards discriminating between burned and unburned classes using M-statistic as separability index and histograms of burn and unburn area. The M-statistic measures class separability defined by Kaufman and Remer[33] as the difference between the means (μ) of two classes burned and unburned normalized by the sum of their standard deviations (σ)[34-37]. The separability index is computed as (Equation 3)[38].

$$\mathbf{M} = \frac{|\boldsymbol{\mu_b} - \boldsymbol{\mu_u}|}{(\boldsymbol{\sigma_b} + \boldsymbol{\sigma_u})} \quad (3)$$

Where, μb and μu are the mean values of the burned and unburned areas, respectively, of the considered SI-difference/weighted fusion difference images, σb and σu are the corresponding

standard deviations. The higher M values demonstrate that the selected method can better discriminate burnt areas from unburnt areas than others. Also, the larger M values indicate low degree of histogram overlap between burn and unburn classes[3].

The final accuracy of all SI/weighted fusion difference images in discriminating the burn scar in the Vidarbha region was assessed by generating error/confusion matrices of the collected ground truth data and by available fire hotspot information. An error matrix is a quantitative approach to characterising image classification accuracy, which is a square array of numbers laid out in rows and columns that shows correspondence (agreement and disagreement) between the classification result and a reference image. Information in the error matrix was evaluated using descriptive evaluation techniques. Using descriptive evaluation, the overall accuracy of classification results can be clearly described, along with the errors of inclusion (commission errors) and exclusion (omission errors)[39,40].

## 3 Results and Discussion

As mentioned in the previous sections, the present study examined month-wise (during fire season) 8 individual spectral indices' difference images, CVA images, and various ensemble images (weighted fused normalized difference images). The results show that SIs difference images of NDVI, NBR, BAI, MSAVI and BAIMS give better outcomes than the other two individual SIs (NDMI & BAIML) and CVAs. However, ensemble images were given far better accuracy than individual SIs difference images (Figure 3).

**Figure 3**

Most of the region in the study area, specifically in forest area, is hilly, where different slopes/aspects and hill shading conditions create lots of spectral mixing with burn scar, making it challenging to delineate the burnt area accurately. Some of the best performers among the group of spectral indices over a particular hilly region are illustrated in Figure 4. NDVI difference image could

map burned patches but could not accurately delineate all the burned patches from unburned area, only the recent burned patches were accurately delineated. Generally, the normalized burn ratio was often considered the best SI, but our study found that it failed to discriminate burned scar from hill shadows (Figure 4b). Although it's ensambling with other group of indices like BAI, BAIMS (Figure 4f) and BAI, MSAVI (Figure 4g) present better discriminated result but still hold some spectral mixing in certain areas. NDMI results were pattern wise similar to NBR but carried even more spectral confusion, possibly because of water-logged or wetland condition, which shows reflectance properties near the burn scar. BAIMS (Figure 4e) outcome was better than other SWIR band SI because it does not contain false burn patches due to spectral confusion but able to detect only highly burnt dense patches with a very low reflectance value. MSAVI (Figure 4d) outcome was very promising, it could even detect coarsely burnt patches because of its ability to minimize soil's high reflectance, making MSAVI very sensitive to low vegetation cover[30]. If we consider only individual SI performance, then BAI (Figure 4c) was the best but gave even better results when ensemble with MSAVI (Figure 4h). The study found that the weighted fusion of BAI, MSAVI and BAIMS (Figure 4i) was superior in discriminating burnt scar.

**Figure 4**

Burn scar extraction was performed using individual SI difference, CVA and weighted fusion difference images through optimal thresholding method. Computed threshold values for some of the difference images are tabulated below (Table 2).

**Table 2**

These computed values were not fixed for different months with in a fire season. Although the same value can be used throughout one fire season but to delineate more accurately, there were slight variations in the selected threshold values. Some of the obtained results are demonstrated in Figure 5.

**Figure 5**

The capabilities of the previously described difference images in exact discriminating between burned and unburned classes were evaluated and compared using the following three approaches. For this, 150 random sample points of burned area were created using ground truth and fire hotspot information, and 150 reference points of unburned area of similar slope/aspect were created in near proximity of respective burned areas. Here, instead of pre-fire values of burned samples, the difference image values of unburned areas are considered as a reference for healthy vegetation.

- Analysis of burned-unburned separability capabilities of difference images, the M-statistic: The higher M values demonstrate that the method can make better discrimination of the burned class than others. Weighted fusion is created with all possible combinations of indices, from which the top few best performers are presented here. As illustrated in Figure 6, CVA performed worst, and the weighted fusion of BAI, MSAVI and BAIMS outcome was superior amongst all examined difference images in discriminating burnt scar.

**Figure 6**

- Histogram of burned and unburned sample points: Figure 7 supports the same presumption: larger M values indicate low degree of histogram overlap between burn and unburn classes. As per this also the weighted fusion of BAI, MSAVI and BAIMS demonstrates the least overlap, hence the best separability of burned classes from unburned classes.

**Figure 7**

- Descriptive evaluation of classified output: Further analysis of the mapping capabilities of SI/weighted fusion difference images includes detailed accuracy assessment quantifying omission and commission errors (Figure 8). As shown by the outcome of the validation process, NBR does not offer good performance in our study, with large number of false alarms (24.52%), even though the percentage of undetected burned patches was less (12.59%). The weighted fusion of BAI, MSAVI and BAIMS performs best, offering 86.61% overall accuracy with 8.12% commission and 10.27% omission error.

**Figure 8**

Limitations of the study: One of the significant limitations of this method is that Pre-fire and postfire images need to be of the same satellite with the same path and row (with sun azimuth and zenith angle same to the maximum extent) to nullify the hill shadow effects. Using the SI differencing this hill shadow is getting removed but if there is a large differences in sun azimuth and zenith angle in Pre-fire and postfire datasets, few patches of hill shadow may still remain, which may get mixed up with burn scar pixels. The unavailability of the same satellite's well-separated (Month wise) cloud-free data may omit some of the small fire scars due to pre-monsoon showers. Moreover, this study can only be replicated in dry deciduous, moist deciduous, grasslands and thorn forests where the leaves will defoliate in the fire season. In the cases of evergreen and semi-evergreen forests, the fire on the forest floor will not get picked up.

## 4 Conclusion

The present study analysed various SI and their weighted fusion to discriminate burned from unburned classes. Separability and accuracy of each of these techniques were evaluated using M-statistic, burn-unburn class distribution and overall accuracy assessment. The result shows that weighted fusion method using BAI, MSAVI and BAIMS was found to be the best suited method for burn scar delineation when compared to individual SIs and other SI combinations. CVA is the least

performer among the various techniques tried. NDVI can be used for burn area extraction if employed immediately after the fire event, when the magnitude of change in vegetation chlorophyll content is highest. Even though some studies have shown that visible and NIR bands are less effective than SWIR for discriminating burned areas, the present study reveals that for partially burned area, indices with visible and NIR seemed to play a more significant role in estimating the burned area accurately. As a result, BAI and MSAVI performed better than NBR, NDMI, BAIML and BAIMS in the delineation of burn scar. However, weighted fusion of BAI, MSAVI and BAIMS offers a very low rate of omission and commission errors with good overall accuracy among all the examined spectral indices and their combinations, especially in hilly regions. The weighted fusion of BAI, MSAVI and BAIMS was found to be the best method in discriminating forest fire scar in the deciduous tropical forest of India, as demonstrated in the present study. The applicability of this technique to other biomes is still to be tested.



**Acknowledgement**

Authors extend their sincere gratitude to Director, National Remote Sensing Centre and Chief General Manager, Regional Centres. The technical support provided by Regional Remote Sensing Centre-Central staff is duly acknowledged. We are also thankful to USGS Earth Explorer maintained by the NASA for online accessibility of Landsat data. Authors are also thankful to the anonymous reviewers for their support in improving the manuscript.

**References**

1. Menon, A.R.R., Varghese, A.O. and Martin Lowel, K.J., Impact of fire on Moist deciduous forest Ecosystem of southern tropical forests of India. In Impacts of Fire and Human Activities on Forest Ecosystems in the Tropics. Pp. 52-61 in proceeding of International Symposium on Asian Tropical Forest Management, Samarinda, Indonesia, 1999.

2. Bright, B.C., Hudak, A.T., Kennedy, R.E., Braaten, J.D. and Khalyani A.H., Examining post-fire vegetation recovery with Landsat time series analysis in three Western North American forest types. *Fire Ecology*, 2019, **15**, 1-14. https://doi.org/10.1186/s42408-018-0021-9.
3. Liu, Y., Dai, Q., Liu, J., Liu, S. and Yang, J., Study of Burn Scar Extraction Automatically Based on Level Set Method using Remote Sensing Data. *PLoS ONE*, 2014, **9**, e87480. https://doi.org/10.1371/journal.pone.0087480.
4. Varghese, A.O., Ecological studies of the forests of Peppara Wildlife Sanctuary using remote sensing techniques. PhD Thesis, Forest Research Institute, Dehradun, 1997, pp. 286.
5. FSI., India State of Forest Report. 2019. https://fsi.nic.in/isfr19/vol2/isfr-2019-vol-ii-west-bengal.pdf. Accessed 6 June 2021.
6. Overpeck, J.T., Rind, D. and Golberg, R., Climate-induced changes in forest disturbances and vegetation. *Nature*, 1990, **343**, 51-53.
7. Roy, P.S., Forest Fire and Degradation Assessment using Satellite Remote Sensing and Geographic Information System. *Satellite Remote Sensing and GIS Applications in Agricultural Meteorology*, 2004, 362-363.
8. Dogra, P., Mitchell, A.M., Narain, U., Sall, C., Smith, R. and Suresh, S., Strengthening Forest Fire Management in India, World Bank, Washington DC, 2018.
9. Varghese, A.O. and Suryavanshi, A., Forest cover transformation analysis and Management of Melghat Tiger Reserve using RS & GIS. NRSC Report: NRSC-RC-REGNAGP-RRSC-NAGP-OCT2020-TR0001690-V1.0, 2017. https://doi.org/10.13140/RG.2.2.27068.49280
10. Parajuli, A., Gautam, A.P., Sharma, S.P., Bhujel, K.B., Sharma, G., Thapa, P.B., Bist, B.S. and Poudel, S., Forest fire risk mapping using GIS and remote sensing in two major landscapes of Nepal. *Geomatics, Natural Hazards and Risk*, 2020, 11(1), 2569-2586. https://doi.org/10.1080/19475705.2020.1853251.

11. Das, J., Mahato, S., Joshi, P.K. and Liou, Y.-A., Forest Fire Susceptibility Zonation in Eastern India Using Statistical and Weighted Modelling Approaches. *Remote Sensing*, 2023, **15**, 1340. https://doi.org/ 10.3390/rs1505134.
12. Varghese, A.O., Mani, J.K. and Jha, C.S., Applications of Geospatial Technology in Forest Resource Assessment, Management, and Monitoring. In: Jha, C.S., Pandey, A., Chowdary, V., Singh, V. (eds) Geospatial Technologies for Resources Planning and Management. Water Science and Technology Library, vol 115. Springer, 2022. https://doi.org/10.1007/978-3-030-98981-1_28.
13. Llorens, R., Sobrino, J.A., Fernández, C., Fernández-Alonso, J.M. and Vega, J.A., A methodology to estimate forest fires burned areas and burn severity degrees using Sentinel-2 data. Application to the October 2017 fires in the Iberian Peninsula. *International Journal of Applied Earth Observation and Geoinformation*, 2021, **95**, 102243. https://doi.org/10.1016/j.jag.2020.102243.
14. Mudi, S., Behera, M.D., Paramanik, S., Jaya Prakash, A. and Prusty, B.K., Recent rise in wildfires in community forests and other natural vegetation: geospatial basis. *Current Science*, 2021, **121**(7), 891-893.
15. Wang, X., Yan, J., Tian, Q., Li, X., Tian, J., Zhu, C. and Li, Q., Estimation of Forest Fire Burned Area by Distinguishing Non-Photosynthetic and Photosynthetic Vegetation Using Triangular Space Method. *Remote Sensing*, 2023, **15**(12), 3115. https://doi.org/ 10.3390/rs15123115.
16. Lee, C., Park, S., Kim, T., Liu, S., Md Reba, M.N., Oh, J. and Han, Y., Machine Learning-Based Forest Burned Area Detection with Various Input Variables: A Case Study of South Korea. *Applied Sciences*, 2022, **12**(19), 10077. https://doi.org/10.3390/ app121910077.
17. Zhao, Y., Huang, Y., Sun, X., Dong, G., Li, Y., and Ma, M., Forest Fire Mapping Using Multi-Source Remote Sensing Data: A Case Study in Chongqing. *Remote Sensing*, 2023, **15**, 2323. https://doi.org/10.3390/ rs15092323.

18. Miranda, A., Mentler, R., Moletto-Lobos, Í., Alfaro, G., Aliaga, L., Balbontín, D., Barraza, M., Baumbach, S., Calderón, P., Cárdenas, F., Castillo, I., Contreras, G., de la Barra, F., Galleguillos, M., González, M. E., Hormazábal, C., Lara, A., Mancilla, I., Muñoz, F., Oyarce, C., Pantoja, F., Ramírez, R., and Urrutia, V., The Landscape Fire Scars Database: mapping historical burned area and fire severity in Chile, *Earth System Science Data*, 2022, **14**(8), 3599–3613. https://doi.org/10.5194/essd-14-3599-2022.
19. Rakholia, S., Mehta, A. and Suthar B., Forest fire monitoring of Shoolpaneshwar Wildlife Sanctuary, Gujarat, India using geospatial techniques. *Current Science*, 2020, **119**(12), 1974-1981. https://doi.org/10.18520/cs/v119/i12/1974-1981.
20. Bar, S., Parida, B.R. and Pandey, A.C., Landsat-8 and Sentinel-2 based Forest fire burn area mapping using machine learning algorithms on GEE cloud platform over Uttarakhand, Western Himalaya. *Remote Sensing Applications: Society and Environment*, 2020, **18**, 100324. https://doi.org/10.1016/j.rsase.2020.100324.
21. Chandel, A., Sarwat, W., Najah, A., Dhanagare, S. and Agarwala, M., Evaluating methods to map burned area at 30-meter resolution in forests and agricultural areas of Central India. *Frontiers in Forests and Global Change*, 2022, **5**:933807. https://doi.org/10.3389/ffgc.2022.933807.
22. Ye, J., Cui, Z., Zhao, F. and Liu, Q., Automated Extraction of Forest Burn Severity Based on Light and Small UAV Visible Remote Sensing Images. *Forests*, 2022, **13**(10), 1665. https://doi.org/10.3390/f13101665.
23. Chuvieco, E. and Congalton, R.G., Mapping and inventory of forest fires from digital processing of TM data. *Geocarto International*, 1988, **4**, 41-53.
24. Martin, M. P. and Chuvieco, E., Cartografía de grandes incendios forestales en la Península Ibérica a partir de imágenes NOAA-AVHRR. *Serie Geográfica*, 1998, **7**, 109-128.

25. Martín, M.P., Gómez, I. and Chuvieco, E., Burnt Area Index (BAIM) for burned area discrimination at regional scale using MODIS data. *Forest Ecology and Management*, 2006, 234. https://doi.org/10.1016/j.foreco.2006.08.248.
26. Key, C.H. and Benson, N.C., The Normalized Burn Ratio (NBR): A Landsat TM radiometric measure of burn severity. U.S. Department of the Interior, Northern Rocky Mountain Science Centre, 1999.
27. Ferna'ndez, A., Illera, P. and Casanova, J. L., Automatic mapping of surfaces aVected by forest Žres in Spain using AVHRR NDVI composite image data. *Remote Sensing of Environment*, 1997, **60**, 153–162.
28. Kasischke, E. and French, N. H., Locating and estimating the areal extent of wildfires in Alaskan boreal forest using multiple-season AVHRR NDVI composite data. *Remote Sensing of Environment*, 1995, **51**, 263–275.
29. Wilson, E.H. and Sader, S.A., Detection of forest harvest type using multiple dates of Landsat TM imagery. *Remote Sensing of Environment*, 2002, **80**, 385–396.
30. Qi, J., Chehbouni, A., Heute, A.R., Kerr, Y.H. and Sorooshian, S., A modified soil adjusted vegetation index. *Remote Sensing of Environment*, 1994, **48**, 119-126.
31. Chuvieco, E., Martin, M.P. and Palacios, A., Assessment of different spectral indices in the red-near- infrared spectral domain for burned land discrimination. *International Journal of Remote Sensing*, 2002, **23**, 5103–5110.
32. Singh, A., Review article digital change detection techniques using remotely-sensed data. *International journal of remote sensing*, 1989, **10**, 989–1003.
33. Kaufman, Y.J. and Remer, L.A., Detection of Forests Using Mid-IR Reflectance: An Application for Aerosol Studies. *IEEE Transactions on Geoscience and Remote Sensing*, 1994, **32**, 672–683.

34. Lasaponara, R., Estimating spectral separability of satellite derived parameters for burned areas mapping in the Calabria region by using SPOT-Vegetation data. *Ecological Modelling*, 2006, **196**, 265–270. https://doi.org/10.1016/j.ecolmodel.2006.02.025.

35. Libonati, R., DaCamara, C.C., Pereira, J.M.C. and Peres, L.F., On a new coordinate system for improved discrimination of vegetation and burned areas using MIR/NIR information. *Remote Sensing of Environment*, 2011, **115**, 1464–1477.

36. Melchiori, A.E., Cândido, P., Libonati, R., Morelli, F., Setzer, A., de Jesus, S.C., Garcia Fonseca, L.M. and Körting, T.S., Spectral indices and multi-temporal change image detection algorithms for burned area extraction in the Brazilian Cerrado. In Proceedings of the Anais XVII Simpósio Brasileiro de Sensoriamento Remoto—SBSR, João Pessoa-PB, Brasil, 25–29 April 2015, 643–650.

37. Smith, A.M.S., Drake, N.A., Wooster, M.J., Hudak, A.T., Holden, Z.A. and Gibbons, C.J., Production of Landsat ETM+ reference imagery of burned areas within Southern African savannahs: Comparison of methods and application to MODIS. *International Journal of Remote Sensing*, 2007, **28**, 2753–2775.

38. Vafeidis, A. and Drake, N., A two-step method for estimating the extent of burnt areas with the use of course-resolution data. *International Journal of Remote Sensing*, 2005, **26**, 2441–2459.

39. Story, M. and Congalton, R. G., Accuracy Assessment: A User's Perspective, *Photogrammetric Engineering and Remote Sensing*, 1986, **52**(3), 397-399.

40. Jenson, J. R., *Introductory Digital Image Processing: A Remote Sensing Perspective*. New Jersey: Prentice Hall, 1995.

**Table 1.** List of spectral indices (SI) used for the study

| Spectral index full name | Equation |
|---|---|
| Burn Area Index (BAI)[24] | $1/(0.1 - Red)^2 + (0.06 - NIR)^2$ |
| Burned Area Index Modified-LSWIR (BAIML)[25] | $1/(0.05 - NIR)^2 + (0.2 - lSWIR)^2$ |
| Burned Area Index Modified-sSWIR (BAIMs)[25] | $1/(0.05 - NIR)^2 + (0.2 - sSWIR)^2$ |
| Normalized Burn Ratio (NBR)[26] | $NIR - lSWIR/NIR + lSWIR$ |
| Normalized Difference Vegetation Index (NDVI)[27,28] | $NIR - Red/NIR + Red$ |
| Normalized Difference Moisture Index (NDMI)[29] | $NIR - sSWIR/NIR + sSWIR$ |
| Modified Soil-Adjusted Vegetation Index (MSAVI)[30] | $(2 \times \mathrm{NIR} + 1) - \sqrt{(2 \times \mathrm{NIR} + 1)^2 - 8 \times (\mathrm{NIR} - \mathrm{Red})}/2$ |
| Here, Blue = visible blue band, Green = visible green band, Red = visible red band, NIR = near infrared band, sSWIR = shorter shortwave infrared band, lSWIR= longer shortwave infrared band. | |

**Table 2.** Threshold values for April 2018 difference images

| **Difference Images** | **Threshold values** |
|---|---|
| NDVI Difference Image | -0.07 to -1.29295 |
| NBR difference image | -0.03 to -1.55056 |
| BAI difference image | -0.07 to -0.964835 |
| MSAVI difference image | -0.0001 to -0.00227939 |
| BAIMS difference image | -0.1 to -4.38848 |
| CVA image | 0.00256489 to $8x10^{-6}$ |
| Weighted fusion difference image of BAI, NBR and BAIMS | -1 to -39.51432 |
| Weighted fusion difference image of BAI, NBR and MSAVI | -1 to -38.7872 |
| Weighted fusion difference image of BAI and MSAVI | -0.5 to -25.6657 |
| Weighted fusion difference image of BAI, MSAVI and BAIMS | -0.4 to -40.84908 |

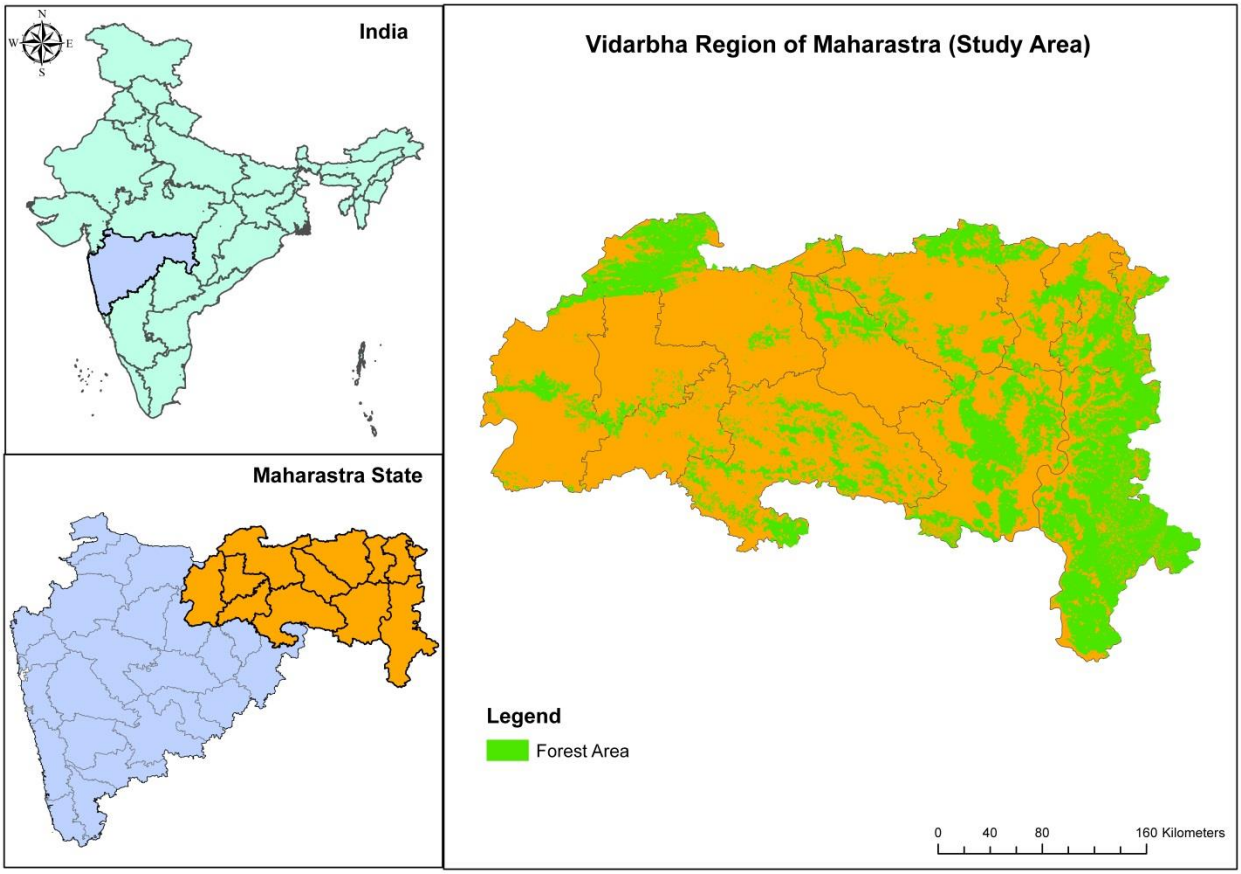


**Figure 1**

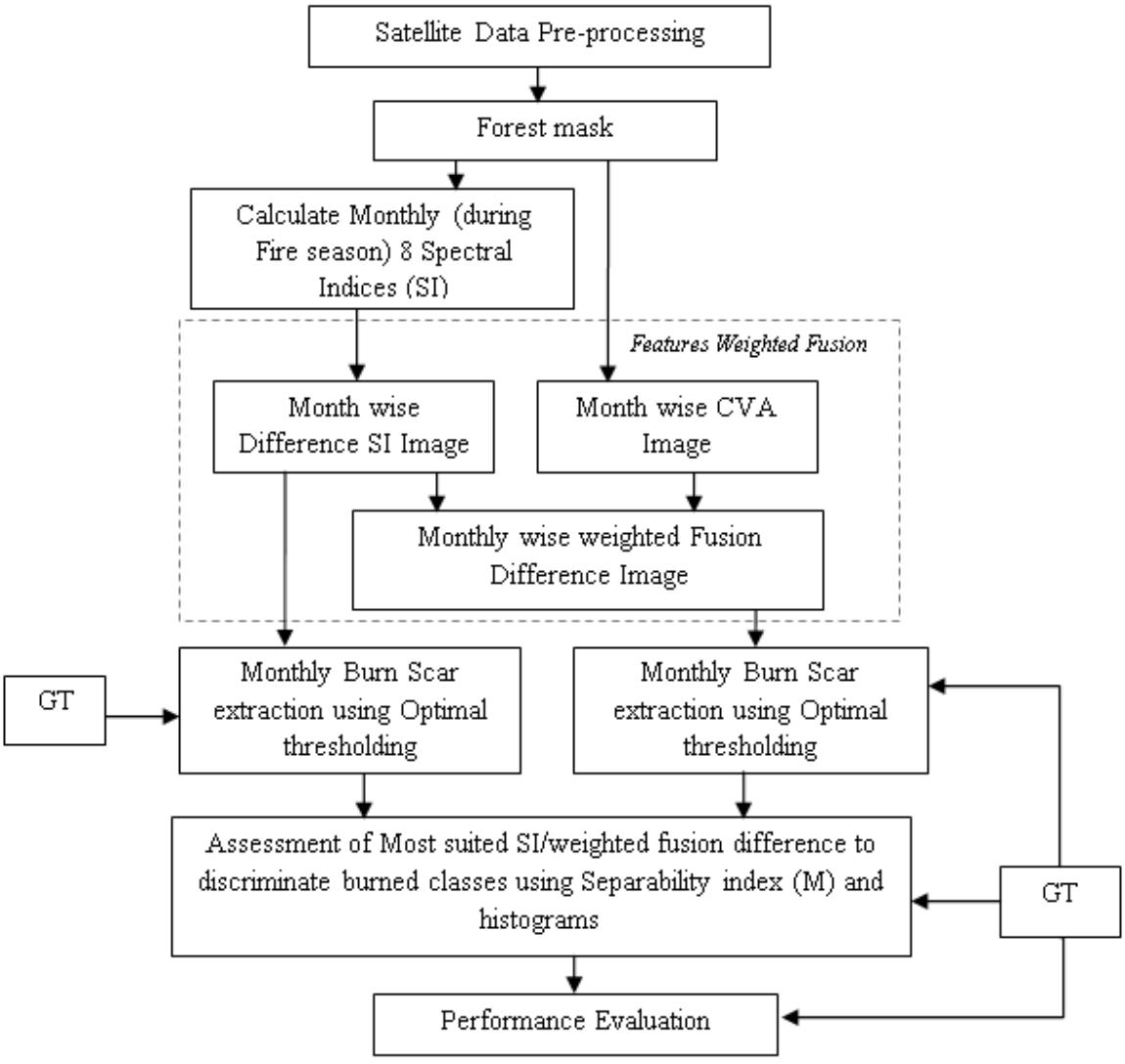


**Figure 2**

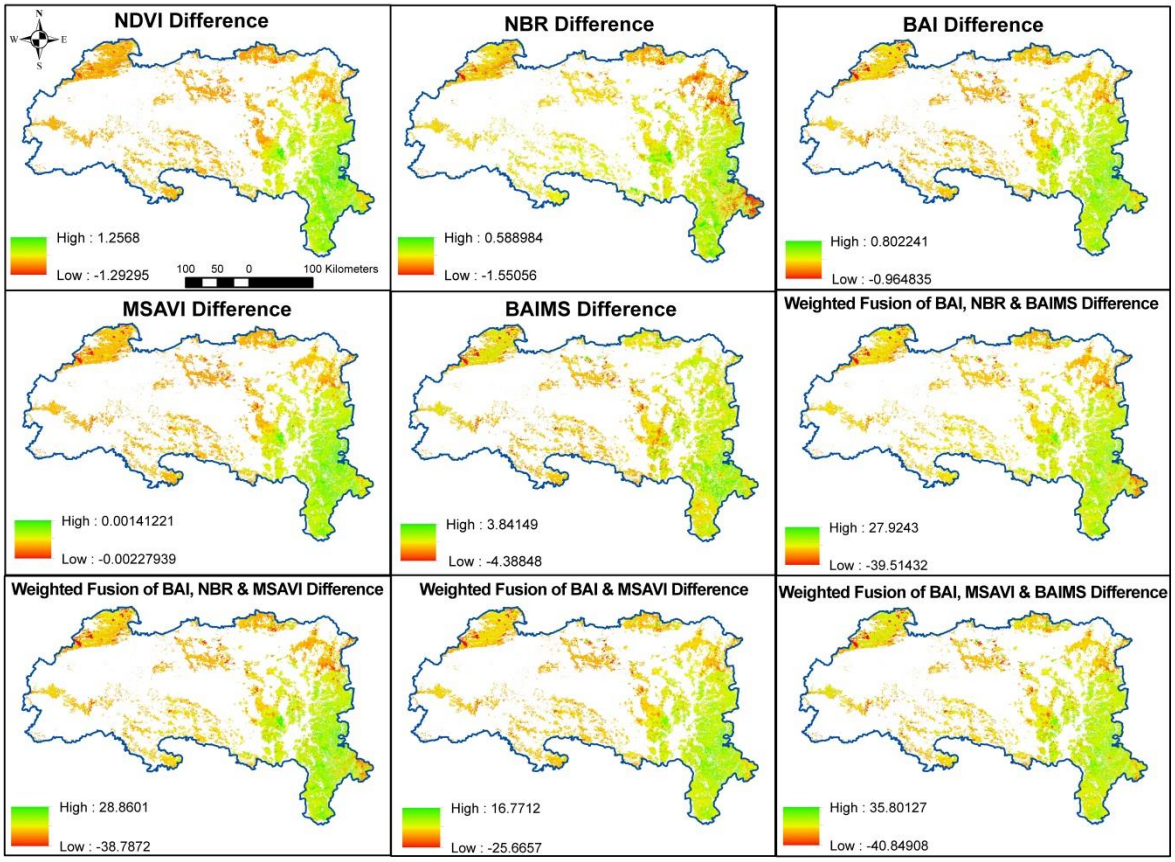


**Figure 3**

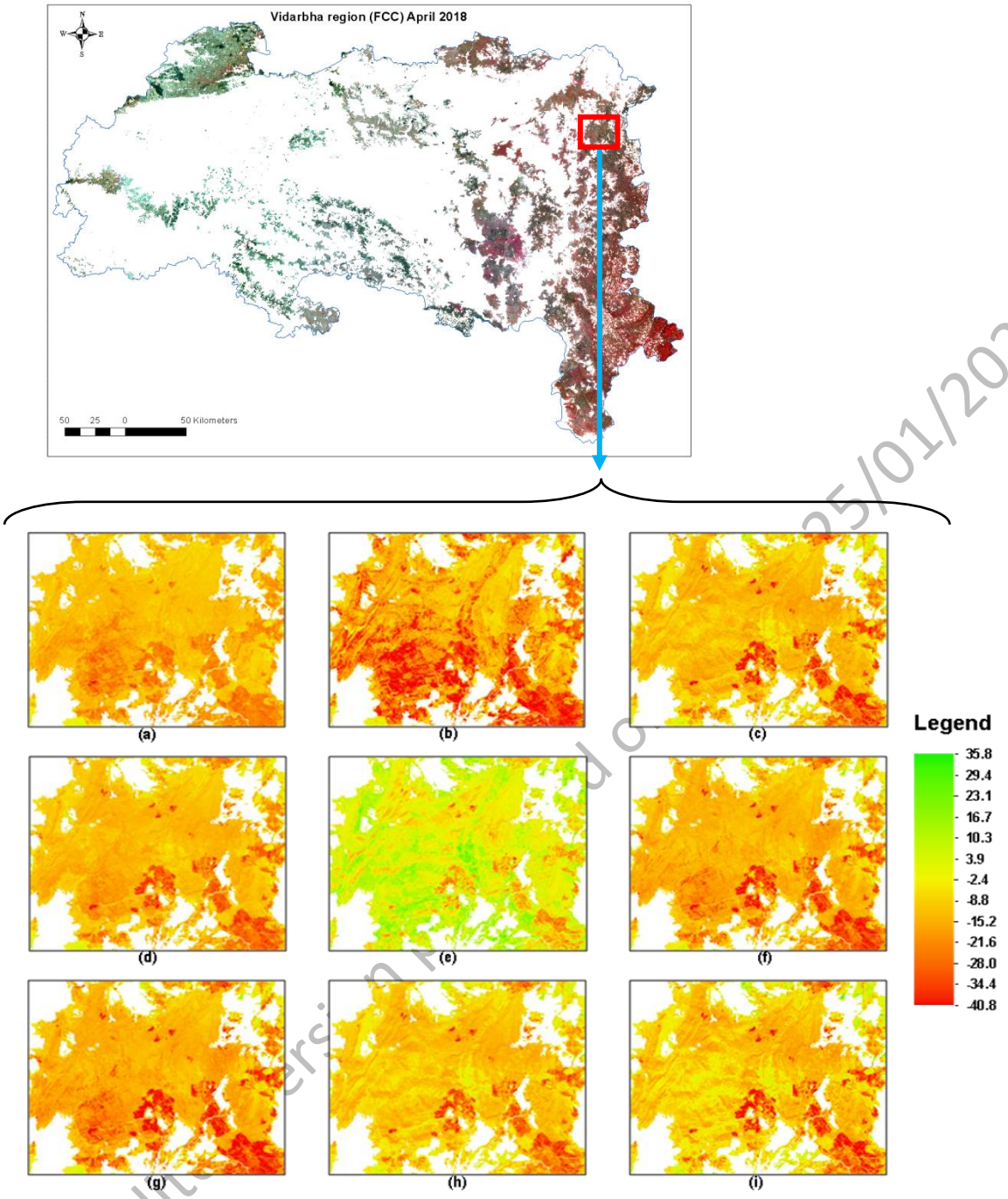


**Figure 4**

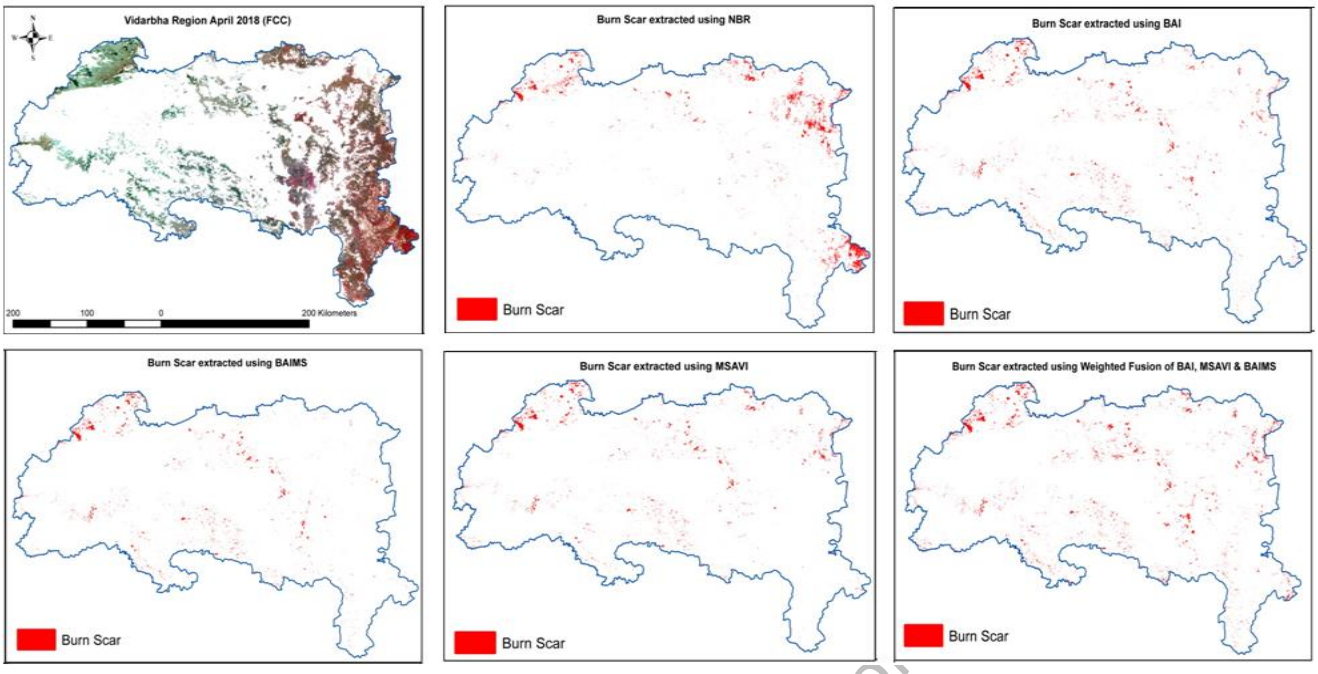


**Figure 5**

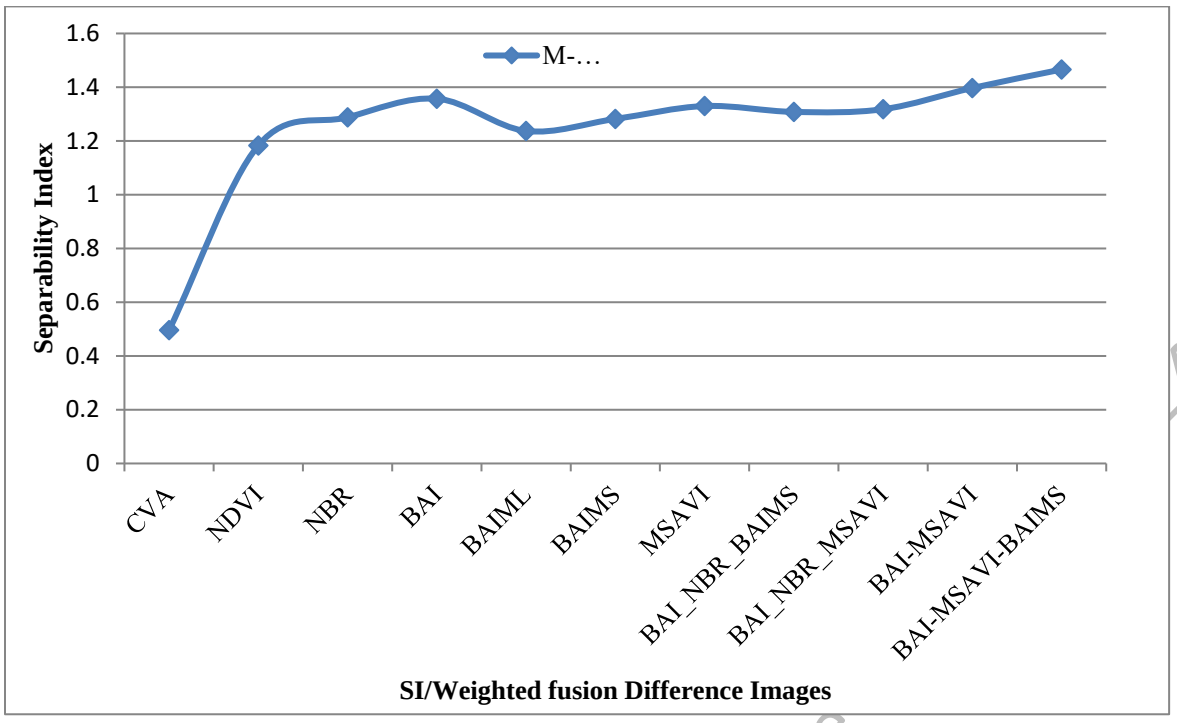


**Figure 6**

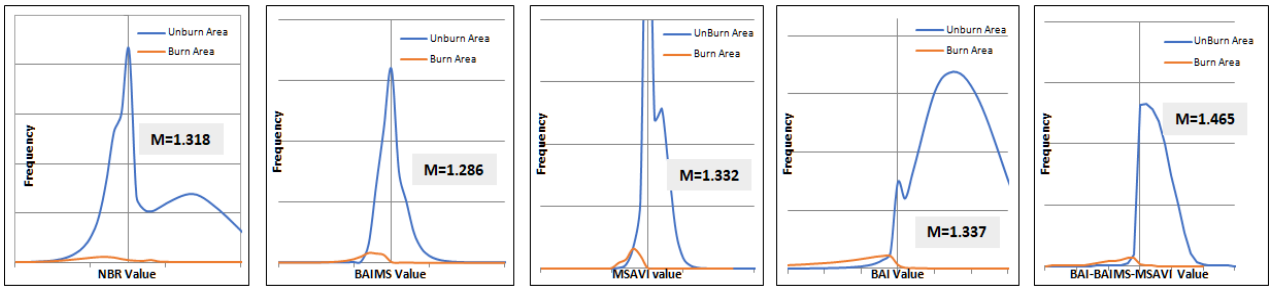


**Figure 7**

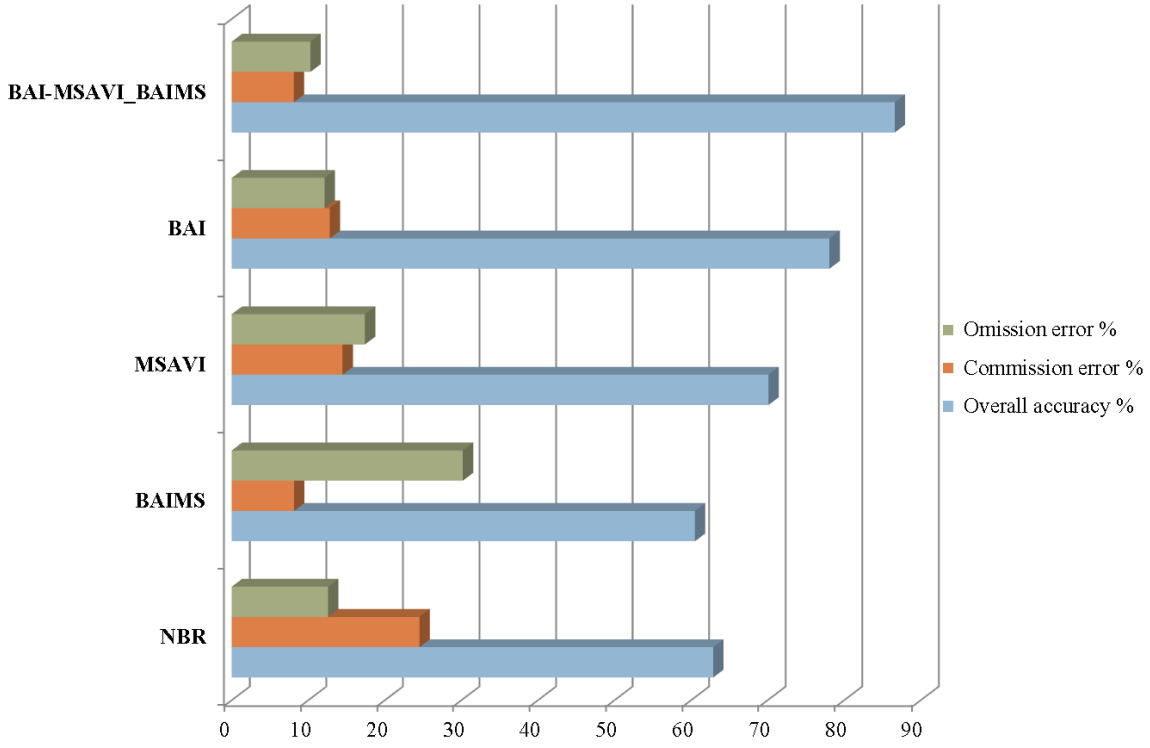


**Figure 8**